

Chemical effects in rare gas adsorption: FLAPW calculations for Ag(001)*c*(2×2)-Xe

Sean Clarke, Gustav Bihlmayer, and Stefan Blügel

Institut für Festkörperforschung, Forschungszentrum Jülich, D-52425 Jülich, Germany

(Received 25 September 2000; published 7 February 2001)

In order to investigate postulated chemical effects in adsorption of heavy rare gas atoms, we investigate the Ag(001)*c*(2×2)-Xe system using the full-potential linearized augmented plane-wave method. Adsorption in the on-top site is found to be favored by 8.6 meV—adsorption in this site suggests that there is a chemical contribution to the bonding. The topology of the charge density associated with the Xe 5*p* states clearly shows that these states are involved in a bonding interaction with the substrate states. We also show that the extra splitting of the 5*p*_{3/2} orbitals arises from adsorbate-adsorbate interactions. It is observed that the spin-orbit interaction drastically alters the electronic, but not geometric, properties of the system.

DOI: 10.1103/PhysRevB.63.085416

PACS number(s): 73.20.At, 68.43.-h

I. INTRODUCTION

The adsorption of inert gas atoms on metal surfaces is an area that has seen a great deal of both experimental and theoretical attention, it is usually considered to be an archetypal example of the van der Waals interaction (an assertion that this paper will to some extent call into question) and so is often used to investigate this interaction. Even though these systems have been extensively investigated, they are still not fully understood and so the aim of this paper is to attempt to answer at least some of those remaining questions in a systematic way using the example of Xe adsorption.

There is work in the literature that calls the assertion that the interaction of inert gas atoms with metal surfaces is a van der Waals interaction into question. In a van der Waals picture of adsorption, one would expect the adsorbate to sit in high coordination sites. However, calculations performed by Müller¹ for Xe on Pt(111) and diffraction experiments by Gottlieb² predicted adsorption in the on-top site. Zeppenfeld *et al.*³ also reported that in scanning tunneling microscopy (STM) experiments for Xe on Pt(111) they observed Xe adatoms forming chains *on top* of step edges. Low-energy electron diffraction (LEED) studies by Narloch and Menzel⁴ and Seyller *et al.*⁵ also found the Xe adsorption site to be the on-top one for Ru(0001) and Cu(111), respectively. These findings do not tie in with a van der Waals picture of inert gas adsorption—the edge of a step is certainly not a high coordination site. These anomalies are explained by assuming that the bonding has some chemical contribution. Eigler *et al.*⁶ found that it was possible to image Xe using the STM, a discovery that they attributed to a charge being transferred from the substrate to the unoccupied Xe 6*s* orbital that is broadened on adsorption and, therefore, overlaps with the Fermi energy thus becoming partially populated. This has been discussed in the literature as a possible bonding mechanism.^{5,7} Müller¹ suggested an alternative mechanism where the charge transfer is from the adsorbate to some unoccupied metal *d* orbitals that sit just above the Fermi energy. Clarke *et al.*⁸ also found evidence of a chemical contribution to the bonding: they calculated the effective charge, which gives a measure of how far the charge state of an atom differs from that of the free atom. They found a negative effective charge on the Xe adsorbate and a corresponding

positive effective charge on the Ag atom sitting below it. They also attributed this to charge transfer due to broadened, unoccupied Xe orbitals overlapping the Fermi energy. In this paper, we attempt to discover whether the ground-state adsorption site for Xe on Ag(001) is the on-top or hollow site, thus allowing us to comment on the likelihood of the interaction having a chemical contribution.

Another question that has seen great interest in the literature is the origin of the extra splitting of the Xe 5*p* levels. The spin-orbit effect splits the 5*p* level of the Xe atom into *j* = 3/2 and *j* = 1/2 components. There is another splitting that occurs when Xe is adsorbed upon a substrate. The 5*p*_{3/2} level splits into *m_j* = ± 1/2 and *m_j* = ± 3/2 components due to the reduction in symmetry on adsorption. Various schemes have been proposed that try to ascertain the mechanism that causes this splitting. Waclawski and Herbst⁹ observed this as a broadening of the 5*p*_{3/2} level for Xe on W(001)—they attributed the broadening to an unresolved doublet that arose from the interaction of the Xe adatom with the W(001) surface crystal field. Antoniewicz¹⁰ then called this into question, pointing out that for the Waclawski-Herbst model to give the correct results, there would have to be an unrealistically large positive charge sitting on the surface ions. He then went on to propose an alternative mechanism for the splitting seen in photoemission experiments. This mechanism was the interaction of the final state ion with its induced image field, an idea that Matthew and Devey¹¹ also put forward. Horn *et al.*¹² performed photoemission experiments studying Xe adsorbed on Pd(001). They also observed a broadening of the Xe 5*p*_{3/2} level that they found to be coverage dependent, this led them to suggest that the splitting is due to a direct lateral interaction. They also made tight-binding calculations of a free-standing Xe monolayer, the electronic structure of this monolayer was in good agreement with the Xe states seen in photoemission experiments.

Henk and Feder¹³ also found evidence to support the idea that lateral interactions make the dominant contribution to the splitting. In calculations based on a fully relativistic Green's-function formalism, they found that the splitting increased as the Xe-Xe separation was decreased and that they could reproduce the experimental photoemission spectrum for Xe/Pt(111) using just a free-standing Xe monolayer. Both of these findings provide strong evidence to support theories

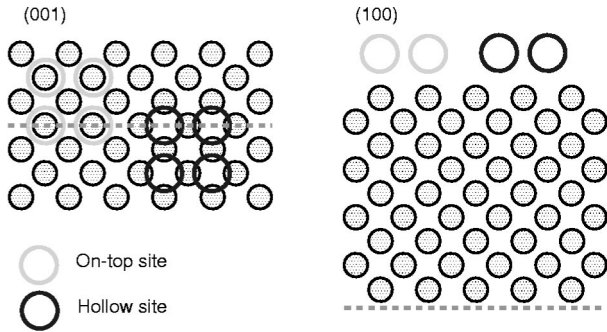


FIG. 1. A schematic view of the two geometries that we used when making our calculations.

based on lateral interactions. Clarke *et al.*⁸ also found evidence that suggests that the splitting occurs mostly from Xe-Xe interactions. They performed calculations for Ag(001) $c(2 \times 2)$ -Xe and reported that the splitting in the density of states was unchanged when the adsorbate layer was displaced into the vacuum.

II. COMPUTATIONAL DETAILS

Our calculations were performed within the density-functional theory using the full-potential linearized augmented plane-wave (FLAPW) method in the film geometry.^{14,15} This method is both accurate and efficient giving excellent results with as few as 100 basis functions per atom. The exchange-correlation functional used was the generalized gradient approximation (GGA) as formulated by Perdew *et al.*¹⁶ We used this because gradient corrections become important for the calculation of the properties of adsorbates due to large charge-density inhomogeneities. The code used to perform these calculations was the FLEUR code, which includes the ability to perform geometry optimizations by calculation of the forces and the total energy and include spin-orbit effects, both of which were necessary for this work.

One of the aims of this paper is to determine which of the adsorbate geometries is the ground state. The energy differences between the different geometries are very small, so a full exploration of convergence with respect to cutoff parameters was necessary, and the calculations were found to be totally converged when using 78 special \mathbf{k} points in the irreducible part of the two-dimensional Brillouin zone¹⁷ with a charge-density cutoff parameter of 12.0 (a.u.)^{-1} and a plane-wave cutoff parameter of 3.6 (a.u.)^{-1} , yielding a basis of 127 linearized augmented plane waves (LAPW's).¹⁸

We modeled the surface by a film consisting of nine layers of Ag with Xe atoms adsorbed on each side. The calculations were performed with the Xe adsorbates in the $c(2 \times 2)$ structure with the adsorbate atom in both the on-top and hollow sites to investigate which site is the ground state (both of these geometries are shown in Fig. 1). The lateral lattice constant of Ag was obtained from a bulk calculation with the same exchange-correlation functional, cutoffs and a comparable \mathbf{k} -point density. The lateral lattice constant obtained from this calculation was 4.15 \AA , a value within 1.4% of the experimental value of 4.09 \AA .¹⁹

III. DETERMINATION OF ADSORPTION SITE

Initially we relaxed a clean Ag(001) surface to get a feel for what (if any) changes the adsorption of Xe made to the surface geometry. These calculations were made without the inclusion of the spin-orbit interaction, as this interaction is only important for the Xe atom. We calculated Δd_{12} , the change in separation between the first and second layer given as a percentage of the bulk interlayer distance, to be $\Delta d_{12} = -1.86\%$ (-0.039 \AA) and between the second and third layer $\Delta d_{23} = 0.68\%$ (0.014 \AA). So, there was very little relaxation with the first layer moving a small amount inwards and the second layer moving outwards by an even smaller amount. This is in qualitative agreement with the experiment^{20,21} and the theory.^{22,23} The fact that these results do not agree quantitatively with the majority of the work in the literature is not a cause for concern, the experimental results have large error bars and our results are reasonable when compared to these error bars. Our work is far more sophisticated than the majority of the theoretical work that exists in the literature. The most sophisticated theoretical works previously carried out were those of Bohnen *et al.*²⁴ (who found $\Delta d_{12} = -1.3\%$ and $\Delta d_{23} = 1.0\%$) and Methfessel *et al.*²³ who found $\Delta d_{12} = -1.9\%$. It is not so surprising that these calculations, which were both carried out within the local-density approximation (LDA), agree so well with our GGA calculations. If calculations of Δd_{ij} are made using a lateral lattice constant that is obtained from a bulk calculation using the same exchange-correlation functional then the results for Δd_{ij} would be expected to be rather insensitive to the choice of exchange-correlation functional.

We then proceeded to perform a geometry optimization of the Ag(001) $c(2 \times 2)$ -Xe system with the adsorbate atoms sitting in both the hollow and on-top positions.²⁵ In these geometries, successive layers alternate between having one and two inequivalent atoms in the surface layer (this is important as we can, in principle, expect different relaxations for each of the inequivalent atoms). In the on-top geometry, there are two inequivalent atoms in the top layer while in the hollow geometry both atoms are equivalent (this situation is reversed in the second layer).

Initially, the adsorbates were placed at a distance roughly equal to the experimental values for the equilibrium distance²⁶ from the surface. However, this initial choice did not need to be especially accurate, as the Xe layer and the topmost two layers of Ag were allowed to relax and the geometry optimized. The results of the calculations are shown in Table I. We see that in the on-top geometry, the Xe-Ag distance is 3.72 \AA , which shows reasonable agreement with the experimental value of $3.5 \pm 0.1 \text{ \AA}$ (Ref. 26), in the hollow geometry the agreement is equally as good with an equilibrium Xe-Ag distance of 3.74 \AA . It is maybe somewhat surprising that we get such good agreement with the experiment as we do not include any special corrections to represent the van der Waals interaction, we use only the GGA of Wang and Perdew.¹⁶ The reason that we get such good agreement was explained by Lang.²⁷ He explained that the essential difference between the LDA (or GGA) and the van der Waals descriptions is the degree of attachment be-

TABLE I. Results of the geometry optimization: d_{Xe} is the perpendicular distance between the Xe atom and the surface layer of silver atoms. In the other rows, Δd_{ij} is defined as the distance from the lowest atom in layer i to the highest atom in layer j measured as a percentage of its difference from the bulk interlayer spacing. Δz_k is the corrugation in layer k , which is defined as being positive if the Ag atom in the unit cell of layer k that sits under the Xe atom is higher than the uncovered Ag atom and otherwise negative. This is measured as a percentage of the bulk interlayer spacing. The calculations were carried out with and without the inclusion of the spin-orbit interaction, the same ground-state geometry was observed in both cases.

| | On top | Hollow | Clean Ag |
|-----------------|--------|--------|----------|
| d_{Xe} | 3.72 Å | 3.74 Å | |
| Δd_{12} | -2.53% | -2.38% | -1.86% |
| Δd_{23} | -0.09% | -0.22% | 0.68% |
| Δz_1 | 0.47% | | |
| Δz_2 | | -0.11% | |

tween the electron and its exchange-correlation hole—in the LDA they are in contact, in the van der Waals treatment, they are completely detached. However, for typical equilibrium adsorption distances of rare gas atoms, in the most important part of the electron orbit (when it is nearest the metal) it lies sufficiently within the electron gas of the substrate for it to be correct to be considered attached to the exchange-correlation hole, and so LDA or GGA functionals are sufficient to give good results.

We see that in the Ag(001) $c(2 \times 2)$ -Xe system, Δd_{12} is larger than for clean Ag. When the Xe is adsorbed in the on-top position, we see that the surface Ag atom that sits underneath the Xe atom does not move as far inwards as the uncovered Ag atom, this is indicative of an attractive chemical interaction between the Xe atom and the atom below it, reducing the inwards relaxation. What is interesting is that Seyller *et al.*⁵ also see this movement of the substrate atom sitting below the Xe atom in their LEED experiments for Xe on Cu(111), but they see the Cu atom moving in the opposite direction to that which we observed. The effect that they observe is much smaller than that which we observe (0.01 ± 0.02 Å) with an error bar that is large enough to put them in agreement with us for the direction. The important thing is that they see a difference in the geometry of the covered and uncovered substrate atoms, thus indicating that the adsorption of inert gas atoms affects the surface geometry.

It is also interesting to note that for the case of adsorption in the hollow site, in contrast with adsorption in the on-top site, it is the Ag atom in the second Ag layer that is not situated underneath the Xe atom that shows the smallest inwards contraction. This supports the idea that hindering of the inwards contraction for the Ag atom situated beneath the Xe adsorbate in the case of adsorption in the on-top site is caused by a some kind of directional bonding that becomes unimportant when we move a layer deeper into the crystal.

For adsorption in the hollow site, we also see that the top Ag layer does not move as far inwards as the uncovered Ag atom is seen to do in the case of adsorption in the on-top site.

TABLE II. $\Delta E = E_{\text{on-top}} - E_{\text{hollow}}$ (per adsorbate atom) as a function of the number of \mathbf{k} points as a test of the \mathbf{k} point convergence. Negative ΔE signifies that on-top site adsorption is favored.

| No. of \mathbf{k} points | ΔE (meV) | |
|----------------------------|------------------|-----------------|
| | No spin orbit | With spin orbit |
| 36 | -8.15 | -8.89 |
| 78 | -8.11 | -8.63 |
| 91 | -8.12 | -8.62 |
| 105 | -8.11 | -8.61 |

This could possibly also be a result of bonding between the adsorbate and top layer of substrate atoms hindering the inwards contraction. This is presumably a weaker interaction, as there is a smaller energetic benefit gained from it, as can be seen from our results for the total energy.

It makes sense that we see this suggestion of directional bonding for on-top adsorption but not for adsorption in the hollow site—one of the conditions for bonding in the on-top site occurring is that there must be some kind of chemical bond, whereas a hollow site equilibrium position is expected for a bare van der Waals interaction. From our calculations we can only really speculate as to the origin of these interactions and so this remains a subject for further investigation.

What is really interesting, at least in the case of bonding in the on-top position, is that we see a suggestion of a directional interaction reminiscent of covalent bonding. This is not what one would expect if the bonding in the system were purely physisorptive and lends credence to the idea that there is a chemical contribution to the bonding in the system. We will return to a discussion of the chemical nature of the bonding later in this paper.

From the results in Table I we also see that Δd_{23} is very small, which means that the principle relaxations take place within the Xe and first two Ag layers, these relaxations do not change the adsorption site, but provide enough energetic benefit to stabilize the system by themselves.

Further calculations were made with the spin-orbit interaction included. In these calculations, the equilibrium positions of the atoms were not altered by the inclusion of the spin-orbit interaction, and no further relaxations were seen. Later in this paper we will discuss the important changes that the spin-orbit effect produces in the electronic structure of this system, here it is clear from our geometry optimizations that the spin-orbit interaction does not induce similar changes in the geometry of the system.

We now consider the results for the total energy obtained from our calculations of Ag(001) $c(2 \times 2)$ -Xe. Table II gives $\Delta E = E_{\text{on-top}} - E_{\text{hollow}}$ as a function of the number of \mathbf{k} points. From these results, we see that for calculations performed with and without the spin-orbit interaction included, on-top adsorption is favored. When no spin-orbit interaction was included, on-top adsorption was favored by 8.1 meV (which corresponds to a temperature of about 100 K). The inclusion of the spin-orbit interaction increased the energetic benefit of on-top adsorption by about 0.5 meV. The calculations were performed with several special \mathbf{k} point sets to ensure suffi-

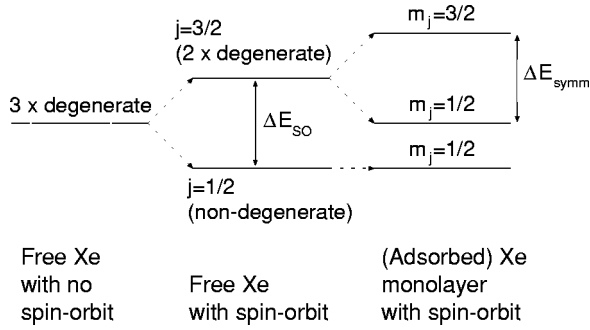


FIG. 2. The splittings that occur in the energy levels of an Xe atom adsorbed on a surface, due to the breaking of symmetry and the spin-orbit interaction.

cient convergence of the total energy because ΔE is such a small quantity. It is clear that ΔE is converged with 78 \mathbf{k} points, but that 36 \mathbf{k} points is a sufficiently large set to use for our force calculations as it still predicts the essential feature that adsorption in the on-top site is favored to the hollow site.

The fact that adsorption in the on-top site is observed is further evidence of some chemical interaction in the system. If the interaction were purely van der Waals in nature, then adsorption in the more highly coordinated hollow site would be expected.

IV. ORIGIN OF THE ADDITIONAL SPLITTING OF THE $5p$ ORBITALS

In a free atom, the Xe $5p$ orbitals split into a nondegenerate $j=1/2$ level and a doubly degenerate $j=3/2$ level due to the spin-orbit interaction. If a monolayer of these atoms were now adsorbed onto a substrate, then the $j=3/2$ level would split into two, an effect caused by the reduction in symmetry on adsorption as shown in Fig. 2; what is not clear is if the effect is caused by interactions between the adatom and the substrate, or by interactions within the adlayer, which is one of the issues that we aim to clear up in this paper.

A useful tool in this discussion is a knowledge of the topology of the charge density associated with each of these states. For a calculation with no spin-orbit effects, at $\bar{\Gamma}$ this is straightforward. If the z direction is perpendicular to the monolayer plane then there is a doubly degenerate $p_{x,y}$ state and a nondegenerate p_z state, with the p_z state being split off from the other two due to the reduction in symmetry introduced by going from a free atom to a monolayer—this splitting is analogous to the splitting that we also see in experiments (and calculations where the spin-orbit interaction is included).

If spin-orbit coupling is included, however, then the situation becomes more complicated. Following Widdra *et al.*,²⁸ for a free atom, the eigenfunctions can be written

$$|3/2, \pm 3/2\rangle = (\pm p_x + ip_y)\chi^\pm / \sqrt{2},$$

$$|3/2, \pm 1/2\rangle = \{(\pm p_x + ip_y)\chi^\mp + 2p_z\chi^\pm\} / \sqrt{6}, \quad (1)$$

$$|1/2, \pm 1/2\rangle = \{(\pm p_x + ip_y)\chi^\mp \mp p_z\chi^\pm\} / \sqrt{3}.$$

This means that in the free atom, for the $|1/2, \pm 1/2\rangle$ state we expect a mixture of p_x , p_y , and p_z character, with each contribution having equal weight. This leads to states that appear to be almost spherically symmetric. For the $|3/2, \pm 3/2\rangle$ state we expect a mixture of p_x and p_y characters leading to states with the characteristic $p_{x,y}$ topology that is well known from atomic physics (a state that is also seen in calculations where we do not include the spin orbit effects). Finally, the $|3/2, \pm 1/2\rangle$ state is a mixture of p_x , p_y , and p_z characters dominated by the p_z contribution, so we would expect this state to resemble a slightly ‘‘fattened’’ p_z orbital.

We approach the problem of discovering the origin of the splitting by making self-consistent calculations for both a monolayer of Xe adsorbed upon the Ag(001) substrate and a hypothetical unsupported Xe monolayer. By comparing the band structures and topology of the states (information that we get via the charge density) in these systems we can investigate the origin of the splitting. We also perform the calculations with and without the spin-orbit interaction so we can at least, to some extent, separate the contributions from the two different mechanisms, and in so doing, simplifying our task.

We begin by considering the band structure of an unsupported Xe monolayer, the geometry of this monolayer is exactly the same as that of the supported monolayer—we simply remove the substrate. Figure 3 shows the band structure for the unsupported Xe monolayer when no spin-orbit interaction is included along with the single state charge-density corresponding to each of the bands at $\bar{\Gamma}$.

We see that the band structure exhibits rather strong dispersion, which suggests that there are strong lateral interactions between the Xe atoms, a fact that we will return to later. We see three bands coming from the $5p$ states,²⁹ which at the high-symmetry points are from the p_x , p_y , and p_z orbitals. At these points p_x and p_y are degenerate, then as we move away from the high-symmetry points, we get linear combinations of p_x and p_y and so we see three nondegenerate bands. From this we can assume that the states highest in energy at $\bar{\Gamma}$ are the doubly degenerate $p_{x,y}$ states and that the state sitting below these is the p_z state (at \bar{M} , this energetic ordering is reversed). This can be clarified further by considering the plots of the charge density of these states lying at $\bar{\Gamma}$, which are given in the insets in Fig. 3. We see that the charge density of the band that is lowest in energy at $\bar{\Gamma}$ clearly has p_z character (this means that it is the band with $m_j=1/2$) and the charge density of the band that is doubly degenerate at $\bar{\Gamma}$ has $p_{x,y}$ character.

The splitting between the $p_{x,y}$ and p_z states is of the order of 0.7 eV, which is larger than splittings reported by other workers in the literature (for Xe adsorbed on a substrate).^{12,30,31} This can be understood by realizing that the splitting increases when the Xe-Xe separation is reduced and the orbital overlap increases³² (which is also evidence that the majority of the splitting is a result of interactions within the overlayer). The Xe-Xe separation that we have used in

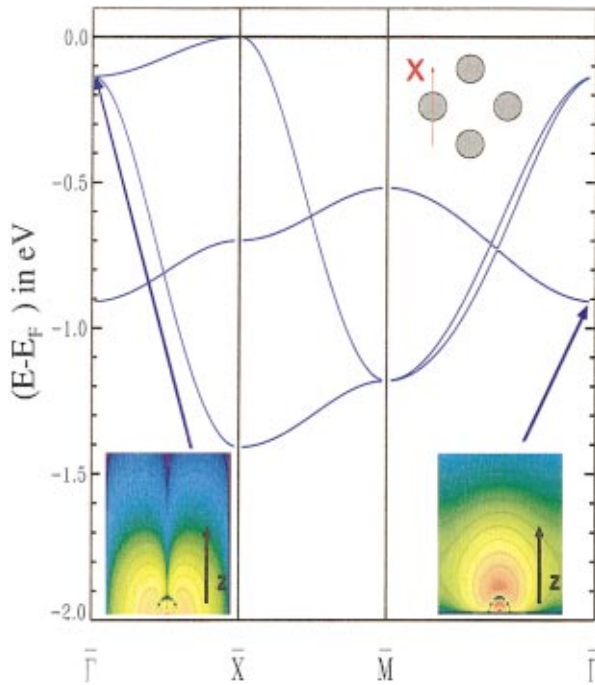


FIG. 3. (Color) The band structure for an unsupported Xe monolayer calculated without spin-orbit effects included at a lattice constant of 4.15 Å . The insets show partial charge densities (for single states) calculated in small energy windows around the bands marked by arrows at $\bar{\Gamma}$. (The plane perpendicular to the surface on which the charge density was evaluated is indicated in the figure.)

our calculations is smaller than any so far reported in the literature as dictated by the lattice constant and overlayer geometry, so it is logical for us to see a larger splitting (especially if we assume that the splitting is dominated by lateral interactions).

We now move on to consider the results of a more realistic calculation for the same system where we include the spin-orbit interaction. If we look at Fig. 4, which shows the single state charge-densities of the Xe 5*p* orbitals at different lattice constants, then, for a lattice constant of 5.20 Å, which approximates the free atom limit, we see orbitals that agree with the picture that was previously described. The state that is lowest in energy at -1.21 eV resembles an *s* orbital and corresponds to the $|1/2, \pm 1/2\rangle$ state, the state at -0.11 eV shows considerable p_z character and is the $|3/2, \pm 1/2\rangle$ state while the state highest in energy sitting at the Fermi energy has $p_{x,y}$ character and so is the $|3/2, \pm 3/2\rangle$ state. We do not present the band structure for the system at this lattice constant, because as one would expect in the free atom limit, it is rather featureless with virtually no dispersion.

If we now consider the system with a lattice constant of 4.15 Å, which is the lattice constant that corresponds to the Xe overlayer structure in the Ag(001)*c*(2×2)-Xe system, we see a somewhat different picture. In the charge density plots in Fig. 4 we see that the state highest in energy still resembles a $p_{x,y}$ orbital, but the orbitals below this have altered quite drastically—the orbital that had largely p_z character now resembles an *s* orbital while the orbital that previously resembled an *s* orbital now seems to have some p_z

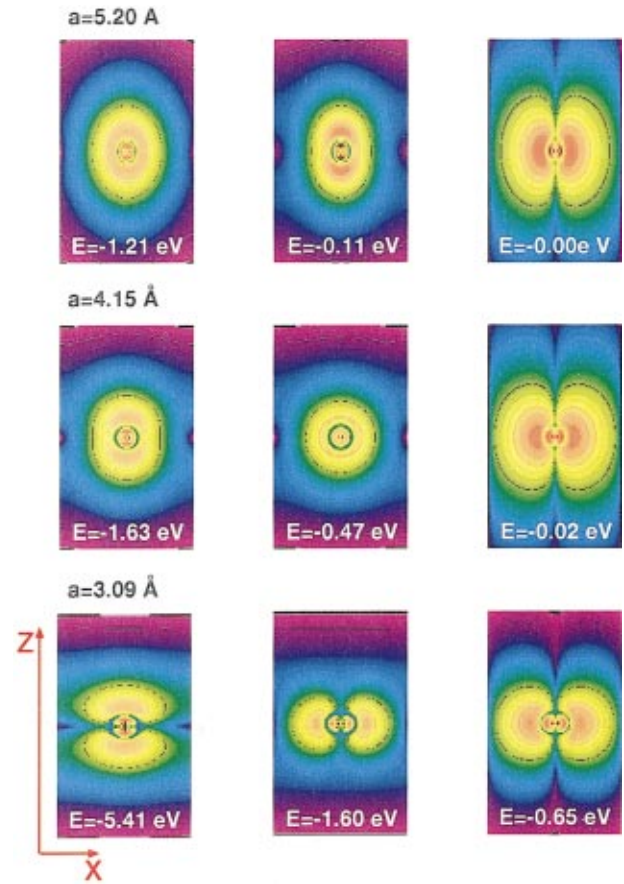


FIG. 4. (Color) Single state charge densities at $\bar{\Gamma}$ for the unsupported Xe monolayer with spin orbit included for the lattice constant that is consistent with adsorption on Ag ($a=4.15$ Å), a stretched lattice constant ($a=5.20$ Å), and a squeezed lattice constant ($a=3.09$ Å). For each value of the lattice constant, the states are ordered with increasing energy from left to right in the figure, with the energies being measured relative to the Fermi energy. The charge densities were evaluated on the same plane as shown in Fig. 3.

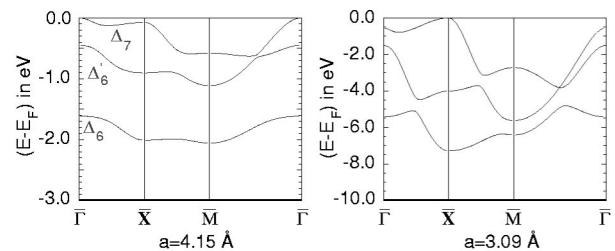


FIG. 5. Band structures for the unsupported Xe monolayer with lattice constants of 4.15 Å and 3.09 Å . The bands for the stretched lattice constant of 5.20 Å are not shown as they are almost completely flat. Between the \bar{M} and $\bar{\Gamma}$ high symmetry points it appears that the upper two bands cross each other. This is not the case; there is actually a very small gap between the two bands.

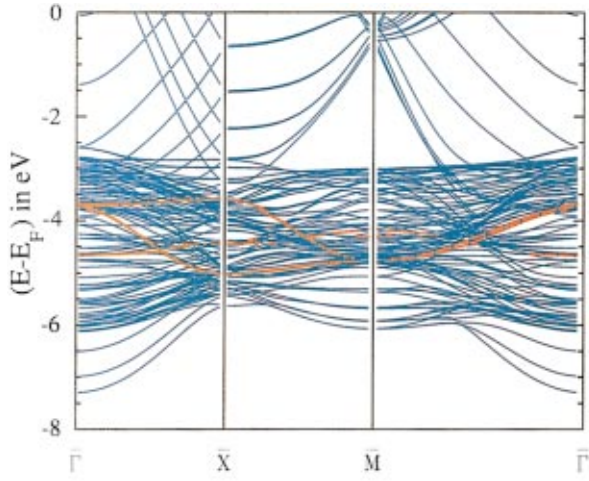


FIG. 6. (Color) The band structure of the $\text{Ag}(001)c(2\times 2)\text{-Xe}$ system (with Xe adsorbed in the on-top position) with no spin-orbit interaction included. The orange bands are those with charge density that is localized by more than 30% in the Xe muffin tins.

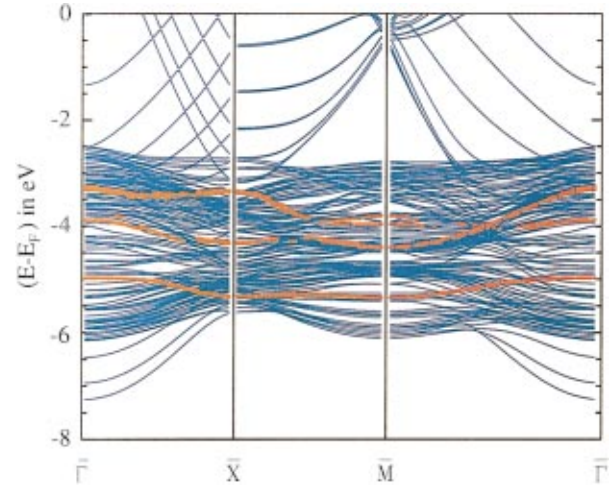


FIG. 8. (Color) The band structure of the $\text{Ag}(001)c(2\times 2)\text{-Xe}$ system (with Xe adsorbed in the on-top position) with spin-orbit coupling included. The orange bands are those with charge density that is localized by more than 30% in the Xe muffin tins.

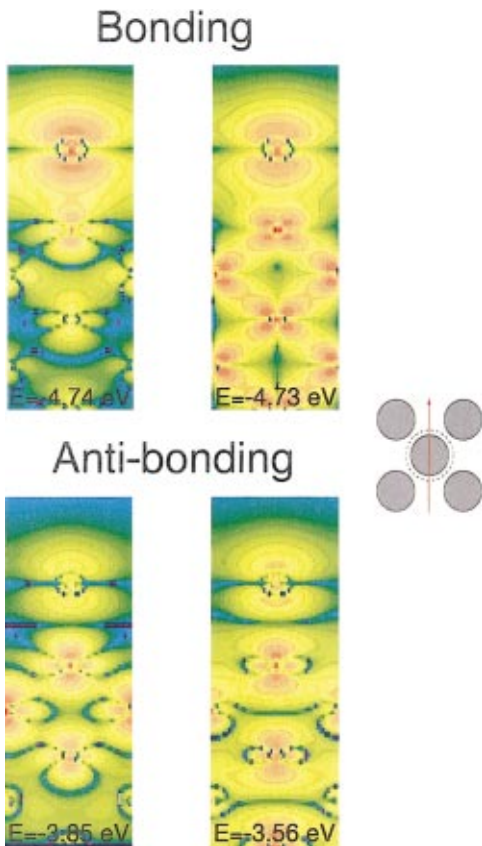


FIG. 7. (Color) Single state charge densities in the $\text{Ag}(001)c(2\times 2)\text{-Xe}$ system (with Xe adsorbed in the on-top position) with the spin-orbit interaction not included calculated at $\bar{\Gamma}$, the plane upon which the charge density was evaluated is shown in the figure. Here we show the pairs of symmetric and antisymmetric states that occur due to Xe atoms on each side of our slab; they do not lie at the same energy due to interactions arising from the finite thickness of the slab.

character. If we look at the band structure given in Fig. 5, we see that there is quite strong dispersion and that along $\bar{M}\bar{\Gamma}$, there appears to be some hybridization between the bands with $j=3/2$. If we now ‘‘squeeze’’ the system to make the lattice constant 3.09 \AA , we see extremely strong dispersion. In fact, this dispersion is so strong that at points away from the high-symmetry points in the Brillouin zone, it is more important than the spin-orbit splitting and so the band structure resembles that obtained for the system with no spin-orbit included with the normal ($a=4.15 \text{ \AA}$) lattice constant. What becomes clear from this is that the symmetry of the orbitals has changed due to the spin-orbit interaction so that bands that were crossing in the band structure with no spin-orbit included avoid crossing when the spin-orbit interaction is included. This occurs as a result of hybridizations that change the topology of the charge density. This can be seen in the plots in Fig. 4 where the topology of the charge densities is almost completely altered. Now the state lowest in energy has a clear p_z character and both the other states have $p_{x,y}$ character.

Let us consider the origin of the hybridizations that occur altering the topology of the charge density. If we ignore spin-orbit coupling, then at $\bar{\Gamma}$ we have a nondegenerate band with Δ_1 symmetry (the p_z orbital) and a doubly degenerate band with Δ_5 symmetry. If we introduce spin-orbit coupling then we have to form the double group, which we do by operating with $D^{1/2}$:

$$\Delta_1 \times D^{1/2} = \Delta_6,$$

$$\Delta_5 \times D^{1/2} = \Delta_6 + \Delta_7. \quad (2)$$

So, the band that had Δ_1 symmetry, which is the lowest in energy at $\bar{\Gamma}$, has Δ_6 symmetry and the doubly degenerate band with Δ_5 symmetry splits into two bands with Δ_6 and Δ_7 symmetry. Let us now consider what consequences this will have. First, as we move the atoms closer together, with

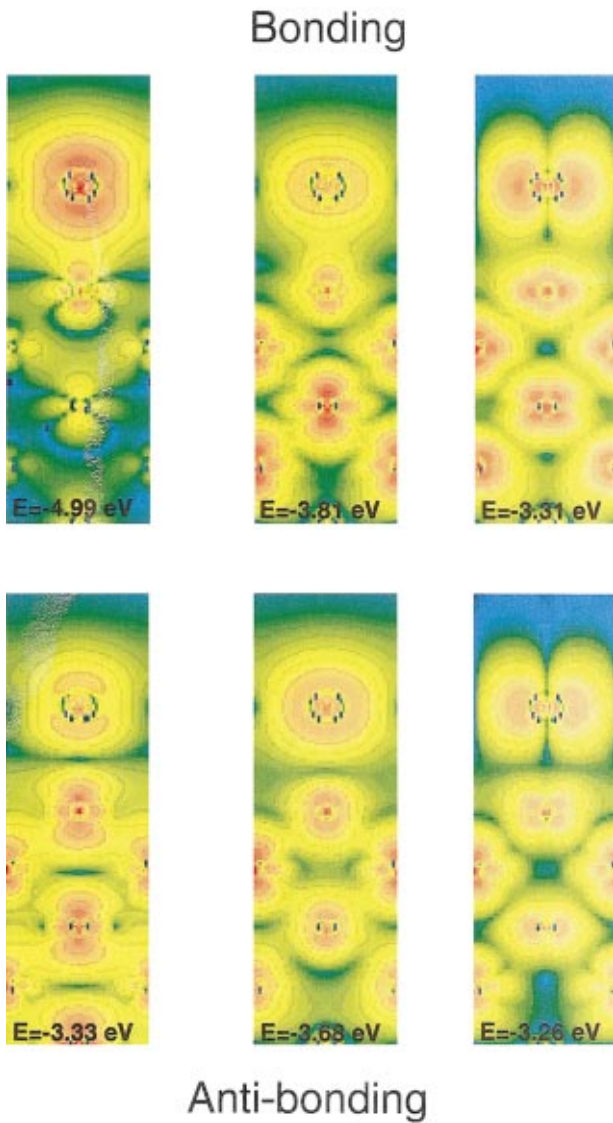


FIG. 9. (Color) Single state charge densities in the $\text{Ag}(001)c(2 \times 2)\text{-Xe}$ system (with Xe adsorbed in the on-top position) with the spin-orbit interaction included calculated at $\bar{\Gamma}$. The states are plotted on the same plane as shown in Fig. 7. Here we do not show the pair of (symmetric and antisymmetric) states arising from the Xe atoms on each side of the slab, but obviously these still exist. The plane on which the charge density was evaluated is oriented the same as that shown in Fig. 7.

ever increasing dispersion, eventually the Δ_6 band lowest in energy will want to cross with the lowest of the other two bands (this is clear from Fig. 5). But symmetry prevents two Δ_6 bands crossing each other so the two bands hybridize and this is the origin of the change in topology of the charge density that is observed. The only thing stopping the band structure of the system with the “squashed” lattice constant in Fig. 5 from looking exactly the same (but with increased dispersion) as the band structure with no spin orbit included, are the modifications to the symmetry arising from the spin-orbit interaction that leads to hybridizations rather than bands crossing. The reason why it is possible for the charge densities of the two states lowest in energy to change as seen

in Fig. 4 becomes clear upon considering Eq. (1). These two states, which are $|3/2, \pm 1/2\rangle$ and $|1/2, \pm 1/2\rangle$ are made up of a combination of p_x , p_y , and p_z ; the hybridizations that occur alter the weight of each of these states in the final state, thus altering the topology of the charge density.

We now consider the $\text{Ag}(001)c(2 \times 2)\text{-Xe}$ system with the Xe atom adsorbed in the on-top site with no spin-orbit interaction. Figure 6 shows the band structure. In this figure we see a typical Ag band structure [for a $c(2 \times 2)$ unit cell], the orange bands in Fig. 6 are those bands with charge density localized in the surface Xe atoms and we see that these bands closely resemble those of the unsupported Xe monolayer as seen in Fig. 3. The single state charge-density plots in Fig. 7, however, are somewhat different in the Xe region to those for the unsupported monolayer.

First of all, we see two states that seem to be associated with Xe p_z states, situated at -4.74 eV and -4.73 eV. The charge density for these two states displays classic signs of bonding behavior with the Xe p_z state hybridizing with the substrate d orbitals leading to a build up of charge between the two atoms. We see two states because of the slab geometry that we use to perform the calculations. We have a slab with a Xe atom on each side of the slab, therefore, we get the same states on each of the Xe atoms, but they are not doubly degenerate because our slab is not infinitely thick, and so, there is some interaction between the two Xe atoms that leads to the formation of linear combinations of their states and a resulting reduction in degeneracy. The slab that we use is basically a quantum well, and so, the Xe states combine to form even and odd states that adhere to the boundary conditions enforced by this well. The splitting is not physical, it is merely an artifact of our chosen computational geometry. The effect, however, does not affect the results, it is a very small effect and just means that one has to be careful when attempting to interpret the eigenvalue spectrum. If we wish to reduce this effect, then we should use a thicker slab with the corresponding computational overheads.

The states at -3.85 eV and -3.56 eV are clearly anti-bonding states with a node in between the adatom and the substrate, we again see the splitting that was previously mentioned but in this case the splitting is larger than before. This is due to the splitting being proportional to the overlap of the even and odd wave functions resulting from the linear combinations that we previously mentioned—if we consider the wave functions associated with bonding and antibonding states, we realize that the bonding states are localized in between the adatom and the substrate whereas the antibonding states are more delocalized and extend further into the slab. This means that the antibonding states have larger weight within the slab, and so, the overlap is larger thus leading to a larger splitting.

If we investigate the $p_{x,y}$ states that are around -3.9 eV, we see the same behavior. We see the formation of bonding-antibonding pairs and these further linear combinations that occur as a result of our geometry. The behavior here is, however, far more complex as here there are not just linear combinations of p_z and metal states but linear combinations of p_x , p_y , and the metal states. We also note that we cannot see the formation of the bonding-antibonding pairs so clearly

and the energetic distance between the bonding and anti-bonding pairs is not so large. This is due to the reduction in overlap between the substrate and adsorbate wave functions due to the topology of the orbitals involved. As a result of this added complexity, it is not straightforward to assign pairs of states to one another, and so, this will not be attempted here; the physics is, however, exactly the same. What we see from the formation of bonding-antibonding pairs is possible evidence of some chemical contribution to the bonding in this system and that the fact that the formation of bonding-antibonding pairs is much stronger for the p_z orbital tells us that if this is indeed evidence of bonding then the bonding orbital on the Xe atom is primarily the p_z orbital and that it is mixing with metal d states. We must be careful, however, from the plots of the charge density of single states, we cannot determine exactly which metal states are mixing with the adsorbate states, we can only say that they are d -like states and so consequently we cannot be sure that this effect is the origin of the bonding.

What we have seen so far seems to support the ideas of Müller,¹ the bonding interaction that occurs causes the Xe $5p$ states charge density as seen in Fig. 7 to become more delocalized due to the interactions with the metal states. What we then see is that the topology of the Xe $5p$ states as they penetrate into the metal resembles the topology of d electrons, which supports Müller's proposed mechanism that the bonding interaction is between Xe $5p$ states and the substrate d electrons.

We now include the spin-orbit interaction in our calculations of Ag(001) $c(2 \times 2)$ -Xe. In the band structure given in Fig. 8, we see that the Xe states (marked by orange crosses) are essentially the same as for the unsupported monolayer (Fig. 5). The spin-orbit effect also makes some limited alterations to the Ag band structure that are most visible for the states closest to the Fermi level. Figure 9 shows selected single state charge densities for the system calculated at $\bar{\Gamma}$. These states were chosen to show states that correspond to the xenon states in the unsupported monolayer shown in Fig. 4. We see that these states closely resemble the ‘‘pure’’ Xe states of the unsupported monolayer but there is once again, as in our calculations without spin-orbit coupling, a clear hybridization effect with the formation of bonding and anti-bonding orbitals. This effect is weak for the state highest in energy that has no p_z character, but we see it is stronger for the two states that have some p_z character. Of these two, the buildup of charge in the ‘‘bond’’ is greatest in the state that has most p_z character. This is consistent with the behavior that we observed when no spin-orbit interaction was applied. We should note that due to the hybridization that occurs between the Xe adsorbate and the Ag states in the substrate, we should not be surprised to see more than the three states that one might naively expect from looking at the Xe bands in the band structure. There are in fact more states involved in the bonding than we show here but we chose the states that had the majority of their weight in the Xe layer for the sake of clarity.

What we also see from the results presented here is, as was the case for the calculations without the spin-orbit inter-

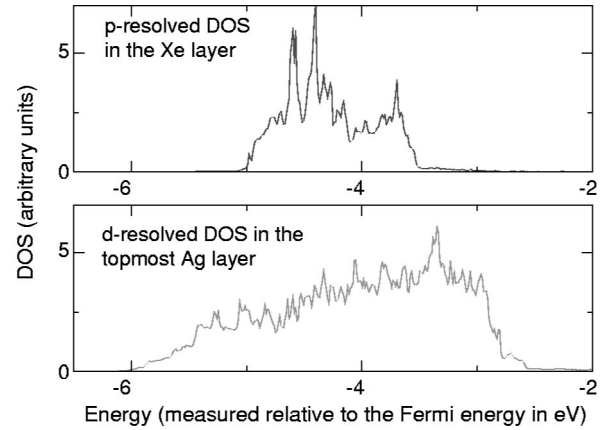


FIG. 10. The density of states in the Xe layer (top) and the topmost layer of the Ag substrate (bottom) calculated using 78 \mathbf{k} points in the irreducible part of the two-dimensional Brillouin zone.

action, that the postulated interaction between the Xe $6s$ state and metallic states is probably not responsible for the chemical nature of the bond. From the single state charge-density plots, it is again clear that the interactions are primarily between the Xe $5p$ states and substrate d electrons, as suggested by Müller.¹ We can see from Figs. 9 and 7 that the metallic d_{z^2} orbital seems to play a prominent role in the bonding mechanism.

If we consider the density of states (DOS) in Fig. 10, we see that in the p -resolved DOS in the Xe layer there is a lot of detail in addition to the Xe $5p$ peaks. This state density is however not near the Fermi energy where there are hardly any states at all and is concentrated lower in energy and seems to come from interactions with the metal d bands, as can be seen from the plot for the d electrons in the top most Ag layer. This is also in agreement with the ideas of Müller.

V. THE MAGNITUDE OF THE SPLITTING OF THE $5p$ ORBITALS

We now proceed to investigate the splittings that we see in the Xe $5p$ orbitals for isolated monolayers and adsorbed monolayers both with and without the spin-orbit interaction. From this we can make an estimate of the splitting that results from spin-orbit coupling, lateral interactions, and from the reduction in symmetry when a surface is introduced. In order to do this, we introduce two quantities ΔE_{Symm} is the distance between the $m_j=1/2$ and $m_j=3/2$ states, ΔE_{SO} is defined as the distance between the states with $j=1/2$ and $j=3/2$, as shown in Fig. 2. Because there is the additional symmetry-induced splitting, ΔE_{SO} is difficult to measure and so we approximate it by measuring the distance between a point halfway between the two symmetry split $m_j=3/2$ states and the $m_j=1/2$ state. We also present the result for ΔE_{SO} from an atomic calculation to justify this approximation.

The results are given in Table III. We see that the results for ΔE_{SO} are consistent with the atomic value of 1.24 eV, we would not expect them to be any closer than they are because of the way that we estimate where to measure the quantity from. When no spin-orbit interaction is included, we get

TABLE III. The splitting of otherwise degenerate energy levels arising from spin-orbit coupling, ΔE_{SO} , and from a reduction of symmetry, ΔE_{Symm} , for a calculation of an unsupported Xe monolayer, a Xe monolayer adsorbed upon Ag(001), and experimental results for Xe monolayers on various substrates at $\bar{\Gamma}$. Experimental data estimated from decomposition of photoemission data into Gaussians as described in the references. ΔE_{SO} measured from half-way between the $m_j=3/2$ and $m_j=1/2$ ($j=3/2$) peaks.

| | ΔE_{Symm} (eV) | ΔE_{SO} (eV) |
|---------------------------|-------------------------------|-----------------------------|
| Atomic Xe | | 1.24 |
| Uns. Mon. (No SO) | 0.77 | |
| Uns. Mon. (SO) | 0.45 | 1.40 |
| Mon. + Subst. (No SO) | 0.92 | |
| Mon. + Subst. (SO) | 0.63 | 1.55 |
| Exp. Xe/Pd(001) (Ref. 12) | 0.57 | 1.42 |
| Exp. Xe/Pd(001) (Ref. 30) | 0.52 | 1.31 |
| Exp. Xe/Pb(111) (Ref. 31) | 0.53 | 1.53 |

rather poor agreement with the experiment for ΔE_{Symm} , but this is improved when this interaction is included. This is not surprising in view of the drastic changes that the spin-orbit interaction induces in the electronic structure of the system. From the results for ΔE_{Symm} it becomes clear that the majority of the symmetry splitting occurs due to lateral interactions. We see this because the splitting seen in the monolayer is almost as large as the splitting seen in the whole system. There is a contribution from the reduction in symmetry that introducing the substrate causes but the effect of the lateral interactions is of the order of three and a half times larger.

So we see that the spin-orbit effect produces the greatest

splitting, this is then followed in importance by the splittings produced by the lateral interaction, and finally, there is a small contribution from the adsorbate-substrate interactions.

VI. CONCLUSIONS

From density-functional theory calculations with the film-FLAPW method using the FLEUR code, we were able to reach a series of conclusions about the adsorption of inert gas atoms. It was clear that the interaction, at least in the case of a large atom such as Xe, is not purely van der Waals, a conclusion that several other workers have previously come to. In addition to this, our results support the mechanism described by Müller, where the bonding interaction is between the Xe $5p$ electrons and the metal d electrons.

By performing total-energy calculations and geometry optimizations, we come to the conclusion that adsorption in the on-top site rather than the hollow site is favored. We also see that, although the spin-orbit interaction drastically alters the electronic structure of the system, it does not effect the geometry of the system.

Finally, we investigated the origin of the splitting of the $5p_{3/2}$ level on adsorption of Xe onto metal surfaces. We came to the conclusion that this was caused by both lateral interactions and substrate-adsorbate interactions with the lateral interactions making by far the dominant contribution.

ACKNOWLEDGMENTS

We thank J. E. Müller and J. E. Inglesfield for useful discussions about the content of this paper. This work was supported by the European Union Training and Mobility of Researchers program (TMR) network Contract No. FMRX-CT98-0178.

- ¹J. E. Müller, Phys. Rev. Lett. **65**, 3021 (1990).
- ²J. E. Gottlieb, Phys. Rev. B **42**, 5377 (1990).
- ³P. Zeppenfeld, S. Horch, and G. Comsa, Phys. Rev. Lett. **73**, 1259 (1994).
- ⁴B. Narloch and D. Menzel, Chem. Phys. Lett. **270**, 163 (1997).
- ⁵Th. Seyller, M. Caragiu, R. D. Diehl, P. Kaukasoina, and M. Lindroos, Chem. Phys. Lett. **291**, 567 (1998).
- ⁶D. M. Eigler, P. S. Weiss, E. K. Schweizer, and N. D. Lang, Phys. Rev. Lett. **66**, 1189 (1991).
- ⁷K. Wandelt and B. Gumhalter, Surf. Sci. **140**, 355 (1984).
- ⁸S. Clarke, M. Nekovee, P. K. de Boer, and J. E. Inglesfield, J. Phys.: Condens. Matter **10**, 7777 (1998).
- ⁹B. J. Waclawski and J. F. Herbst, Phys. Rev. Lett. **35**, 1594 (1975).
- ¹⁰P. R. Antoniewicz, Phys. Rev. Lett. **38**, 374 (1977).
- ¹¹J. A. D. Matthew and M. G. Devey, J. Phys. C **9**, L413 (1976).
- ¹²K. Horn, M. Scheffler, and A. M. Bradshaw, Phys. Rev. Lett. **41**, 822 (1978).
- ¹³J. Henk and R. Feder, J. Phys.: Condens. Matter **6**, 1913 (1994).
- ¹⁴M. Weinert, E. Wimmer, and A. J. Freeman, Phys. Rev. B **26**, 4571 (1982).
- ¹⁵E. Wimmer, H. Krakauer, M. Weinert, and A. Freeman, Phys. Rev. B **24**, 864 (1981).
- ¹⁶J. P. Perdew, J. A. Chevary, S. H. Vosko, K. A. Jackson, M. R. Pederson, D. J. Singh, and C. Fiolhais, Phys. Rev. B **46**, 6671 (1992).
- ¹⁷However, for our purposes convergence was found to be sufficient with 36 \mathbf{k} points.
- ¹⁸Calculations performed with larger charge density and plane wave cutoffs showed no improvement in convergence.
- ¹⁹N. W. Ashcroft and N. Mermin, *Solid State Physics* (Saunders, Philadelphia, 1976).
- ²⁰H. Li, J. Quinn, Y. S. Li, D. Tian, F. Jona, and P. M. Marcus, Phys. Rev. B **43**, 7305 (1991).
- ²¹H. L. Meyerheim, S. Pflanz, R. Schuster, and I. K. Robinson, Z. Kristallogr. **212**, 327 (1997).
- ²²A. M. Rodríguez, G. Bozzolo, and J. Ferrante, Surf. Sci. **289**, 100 (1993).
- ²³M. Methfessel, D. Hennig, and M. Scheffler, Phys. Rev. B **46**, 4816 (1992).
- ²⁴K. P. Bohnen, Th. Rodach, and K.-M. Ho, in *The Structure of Surfaces III*, edited by S. Y. Tong and M. A. van Hove (Springer, New York, 1991).
- ²⁵When making our geometry optimization calculations, we initially optimized the geometry without the inclusion of the spin-

orbit interaction. Then, once we had a ground-state geometry for the system, we performed a new geometry optimization beginning from this geometry with the spin-orbit interaction included. For both the on-top and hollow geometries we observed no further changes in the geometry after the inclusion of the spin-orbit interaction.

²⁶P. I. Cohen, J. Unguris, and M. B. Webb, *Surf. Sci.* **58**, 429 (1976).

²⁷N. D. Lang, *Phys. Rev. Lett.* **46**, 842 (1981).

²⁸W. Widdra, P. Trischberger, and J. Henk, *Phys. Rev. B* **60**, R5161

(1999).

²⁹We do not mention the $5s$ states in our discussions in this paper, as in our calculations they sit typically at about 16 eV below the Fermi energy and, therefore, do not play an important role in the physics that we are investigating. It must, however, be stressed that they are included in our calculations.

³⁰K. Wandelt and J. E. Hulse, *J. Chem. Phys.* **80**, 1340 (1984).

³¹K. Jacobi, *Phys. Rev. B* **38**, 5869 (1988).

³²S. Clarke, Ph.D. thesis, University of Wales Cardiff, 1999.